The Astrophysical Journal Supplement Series, 246:5 (8pp), 2020 January https://doi.org/10.3847/1538-4365/ab5f0a

Nonlinear Convergence of Solar-like Stars Chromospheres Using Millimeter, Submillimeter, and Infrared Observations

F. Tapia-Vázquez[1] and V. De la Luz[2]
[1] Instituto de Radioastronomía y Astrofísica, Universidad Nacional Autónoma de México, P.O. Box 3-72, 58090, Morelia, Michoacán, Mexico
vdelaluz@enesmorelia.unam.mx
[2] Escuela Nacional de Estudios Superiores Unidad Morelia, Universidad Nacional Autónoma de México, Morelia, 58190, Mexico
Received 2019 September 12; revised 2019 November 26; accepted 2019 December 3; published 2020 January 6

Abstract

In this work, we present a new methodology to fit the observed and synthetic spectrum of solar-like stars at millimeter, submillimeter, and infrared wavelengths through semiempirical models of the solar chromosphere. We use the Levenberg–Marquardt algorithm as a Nonlinear method, PakalMPI as the semiempirical model of the solar chromosphere, and recent observations from the Atacama Large Millimeter/submillimeter Array of Alpha Centauri A as a test case. Our results show that we can use solar chromospheric semiempirical models as an input model to reproduce the observed spectrum of solar-like stars. The new profiles show similarities to the solar chromosphere as a minimum of temperature (without the restriction from CO emission) and a plateau in the high chromosphere. Our method provides a new fast numerical tool to estimate the physical conditions of solar-like stars.

Unified Astronomy Thesaurus concepts: Quiet solar chromosphere (1986); Stellar chromospheres (230); Millimeter astronomy (1061); Submillimeter astronomy (1647); Astronomical models (86); Solar electromagnetic emission (1490); Far infrared astronomy (529); Algorithms (1883)

1. Introduction

The particular characteristics of the emission at millimeter, submillimeter, and infrared wavelengths in the solar chromosphere allow us to estimate their temperature and density using indirect methodologies like semiempirical models (Vernazza et al. 1981; Fontenla et al. 1993; Avrett & Loeser 2008). These models are an important tool for a wide set of studies, e.g., solar and stellar chromospheres (Loukitcheva et al. 2004; Linsky 2017), temperature minimum (Liseau et al. 2013; De la Luz et al. 2014), solar flares (Machado et al. 1980; Trottet et al. 2015), and Sun component features (Fontenla et al. 2006).

In terms of solar atmospheric temperatures, the semiempirical models predict values close to photospheric temperatures that decrease until a minimum, then increase dramatically until the coronae (Vernazza et al. 1981; Avrett & Loeser 2008) in a thin layer of around 2200 km. This layer is known as the solar chromosphere. The chromosphere remains observable by different spectral ranges that include ultraviolet in the continuum and line emission, in the visible (mainly Hα), and in the millimeter, submillimeter, and infrared wavelengths. This last wavelength range becomes more important as improvements in the sensitivity and space resolution in modern radio telescopes are made (Nakajima et al. 1995; Kudaka et al. 2015; Wedemeyer et al. 2016).

The process to compute an atmospheric model begin with testing the initial conditions of a semiempirical model (Vernazza et al. 1976; Carlsson 1992; Dere et al. 1997; De la Luz et al. 2010). The process includes three steps: (i) small modifications in an initial temperature profile; (ii) computing the density and pressure required to guarantee hydrostatic, hydrodynamic, or magnetohydrodynamic equilibrium; and (iii) computing the synthetic spectrum to compare with observations. Differences between synthetic and observed spectrum are solved by making changes in the atmospheric temperature profile at different altitudes until synthetic and observed spectrum converges. The number of iterations to converge both observations and the synthetic spectrum restrict the precision of the computation.

Recent observations at sub-mm wavelengths of Solar-like stars for the first time allow for computing the stellar atmosphere at chromosphere altitudes using the solar chromospheric by millimeter-infrared wavelength range observations as a starting model (Liseau et al. 2016). However, the differences between the solar chromosphere and the structure of the atmosphere of Solar-like stars requires thousands of iterations to fit observations and the synthetic spectrum.

In this work, we present a new nonlinear model to converge automatically observed and synthetic spectrum of solar-like chromospheres at millimeter–infrared wavelengths. We used the Levenberg–Marquardt (LM) method to fit observations and synthetic spectrum using PakalMPI as the parametric function (De la Luz et al. 2011). The LM algorithm use three parameters: a set of points in the electromagnetic spectrum as the independent variable (ν) in the LM scope, PakalMPI as the function model ($f(\nu, T_r)$), and the temperature model (T_r) as a set of discrete points used to compute

$$T_b = f(\nu, T_r), \tag{1}$$

where T_b is the synthetic spectrum. In our case, the observed spectrum that corresponds with the frequencies is the dependent data (T_b^o). Our model does not take into account limb brightening contribution. We compute the brightness temperature in the center of the stellar disk.

In Section 2 ,we present the region of the spectrum under study (an independent variable). In Section 3 we present our parametric semiempirical model PakalMPI (the function model). In Section 4 the set of observations of Solar-like stars are used as test cases (dependent data). In Section 5, we describe the general approximation and restriction of the LM method used in this work. In Section 6, we show the results of

the case test. Finally, in Section 7, we present our discussion and conclusions.

2. The Independent Variable: The Millimeter, Submillimeter, and Infrared Wavelengths

The independent variable in the LM scope represents the set of data that are evaluated in the function model. In this work, the independent variable (ν) is a set of frequencies of the electromagnetic spectrum at millimeter, submillimeter, and infrared wavelengths:

$$\nu = \{\nu_1, \nu_2, \ldots, \nu_k\}, \quad (2)$$

where k is the number of points in the observed electromagnetic spectrum and ν_i is the central frequencies of radio observations constrained to cover the 10 bands by the Atacama Large Millimeter/submillimeter Array (ALMA, from 35 to 950 GHz) and *Spitzer* (12.5 THz):

$$35\ \text{GHz} \leqslant \nu_i \leqslant 12.5\ \text{THz}.$$

This range of frequencies allow us to use the tomographic properties of the emission to estimate the radial temperature and the density profile evolved in the synthetic electromagnetic spectrum (De la Luz 2016).

3. The Parametric Function Model: PakalMPI

LM requires a function model that receives the independent variable (ν) and a set of parameters (T_r) that fit the model (Equation (1)). In our case, we modify PakalMPI model (De la Luz et al. 2010, 2011) to work as a parametric function. PakalMPI model uses Bremsstrahlung (Dulk 1985; Güdel 2002), inverse Bremsstrahlung (Golovinskii & Zon 1980), and H- (Zheleznyakov 1996) mechanisms as a source of opacity. However, Bremsstrahlung and H- are the most important mechanisms of thermal emission in the chromosphere (De la Luz et al. 2011).

The set of parameters are temperature points that represent the radial temperature profile under study:

$$T_r = \{T_1, T_2, .., T_n\},$$

where n is the number of altitudes in the radial temperature profile and T_i is the ordered radial temperatures against distance over the photosphere from a semiempirical model. We used the C7 model (Avrett & Loeser 2008) as an initial condition (the radial temperature and density) because it is a consistent model of the solar chromosphere especially on the temperature minimum (De la Luz et al. 2014). The C7 model is a one-dimensional and time-independent model of the average quiet Sun. This model replaced the earlier model C of Vernazza et al. (1981) and takes into account observations of the extreme ultraviolet spectrum and two measurements in the submillimeter region to get a good average of the temperature minimum. However, this model does not reproduce the observations in the submillimeter, millimeter, and radio range correctly (De la Luz 2016). De la Luz et al. (2014) showed that by modifying the temperature profile, it is possible compute a better fit in this region of the spectrum. The new model obtained was compatible with the theory presented by Avrett & Loeser (2008).

The temperature profile passed as arguments together with the frequency ranges to PakalMPI. Then, PakalMPI computed the synthetic spectrum in three steps: (i) compute a new radial density profile iteratively using the radial temperature profile to satisfy the hydrostatic equilibrium, (ii) compute the ionization stages of a set of atoms that represents the chemical composition of the atmosphere, and (iii) solve the radiative transfer equation in the set of requested frequencies. The two last steps can be computed in parallel using the Message Passing Interface (MPI) methodology. Detailed information about the steps can be found in De la Luz et al. (2010).

PakalMPI output includes the synthetic spectrum, the radial profiles of all the ions, temperature, density, and the pressure of the atmosphere in equilibrium. This output is used in further steps of our methodology.

4. The Dependent Data: Observations of Solar-like Stars at Millimeter, Submillimeter, and Infrared Wavelengths

In this work, the dependent variable is represented by the observed spectrum:

$$T_b = \{T_b^{\nu_1}, T_b^{\nu_2}, \ldots, T_b^{\nu_k}\}, \quad (3)$$

where $T_b^{\nu_k}$ is a observed point in the electromagnetic spectrum.

The development of new infrastructure (ALMA, the Large Millimeter Telescope, etc.) allows us to study main-sequence stars in mm—sub-mm regime. The emission at these wavelengths originated in the chromosphere mainly to free–free emission (Dulk 1985; Loukitcheva et al. 2004; Wedemeyer et al. 2016), and neutral interaction (Zheleznyakov 1996) but in general, it is not well-constrained (Cranmer et al. 2013). The first binary stellar system that has been observed and studied in this regime has been Alpha Centauri (α Cen) located at 1.3384 $\pm$ 0.0011pc (Kervella et al. 2017). The system α Cen is composed of two stars: α Cen A (G2 V) and α Cen B (K1 V). In both, the minimum temperature was observed by Liseau et al. (2013) in the far infrared. Liseau et al. (2016) showed that an atmospheric structure similar to the Sun can be adapted to solar-like stars.

In order to test our model, we have chosen α Cen A since it is often considered a solar twin (Cayrel de Strobel 1996) and has observations from the far-infrared to the millimeter range (Liseau et al. 2016).

5. LM Approach: The KP Model

There are several implementations of the LM algorithm (Marquardt 1963; Press et al. 1986; Pujol 2007). In this work, we use least square fit (LsqFit) package developed by Julia Optim team (Mogensen & Riseth 2018).

The model that we present in this work is called Kinich–Pakal (KP). The aim of KP is to compute the best model of the stellar atmosphere to fit the synthetic spectrum to observations at millimeter, submillimeter, and infrared wavelengths.

In Figure 1, we show the pseudo code of KP. We start reading the initial conditions of a single model that includes: the radial temperature, hydrogen density, and pressure. KP reads the radial profiles and the observations and start the computations iteratively using PakalMPI as a function model.

In each iteration, KP computes the hydrostatic equilibrium of the input atmosphere and computes their synthetic spectrum. The computations of the synthetic spectrum are performed in

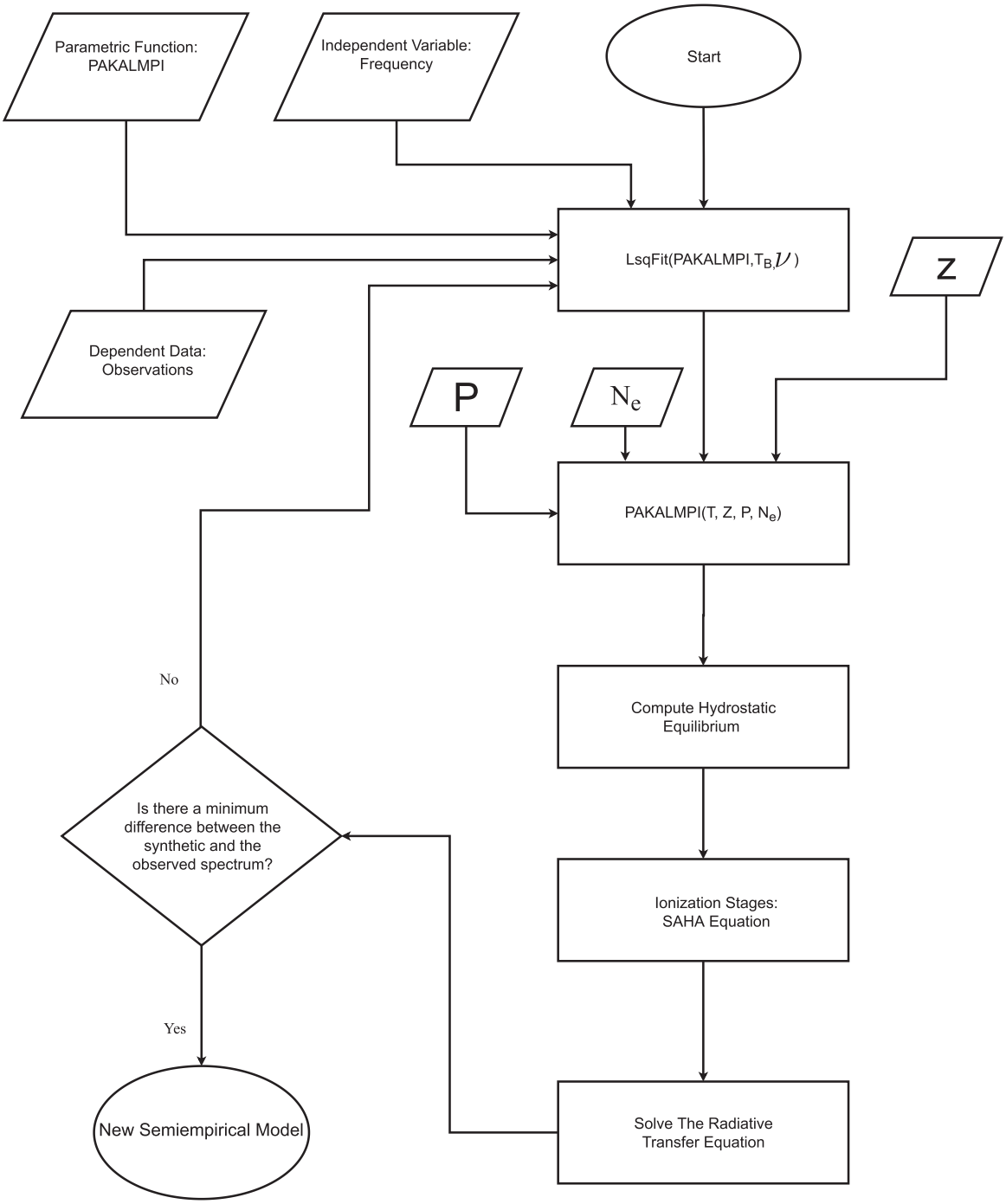

Figure 1. Diagram of operation for KP. KP uses a parametric function (PakalMPI), a set of dependent data (observations), and independent variables (frequency) as inputs. The LsqFit function starts the LM algorithm. PakalMPI computes the hydrostatic equilibrium and solves the radiative transfer equation. LM receives the computed spectrum from PakalMPI and compares it with observations. If the error is higher than the predefined δ, then LM modifies the temperature profile and repeats the process. If the error is less than δ, then KP produces a new semiempirical model.

parallel for each frequency. If the differences between the observed and the synthetic spectrum are greater than an epsilon stop flag, then the computed atmosphere becomes the initial condition for the next iteration and the process continues to step forward.

KP has several flags that constrain the LM method. The constraints include: setting the global limits of the solution, limiting the solution in a defined range, and the absolute error tolerance against the set of observations. The performance of KP depends of the flag constraints and is studied in the following section.

6. Test Case: α Centauri A

α Cen A and B were the first stellar system resolved in the submillimeter wavelength by ALMA (Liseau et al. 2015). Table 1 shows the properties of the observations of α Cen A during Cycle 2 of ALMA between 2014 July and 2015 May. In

Table 1
ALMA Brightness Temperatures for α Cen A from Liseau et al. (2016)

Wavelength (mm)	Frequency (GHz)	Facility	Flux (mJy)	Brightness Temperature (K)
3.075	97.5	ALMA Band 3	3.33 ± 0.01	8618 ± 31
2.068	145	ALMA Band 4	6.33 ± 0.08	7316 ± 88
1.287	233	ALMA Band 6	13.58 ± 0.08	6087 ± 36
0.873	343.5	ALMA Band 7	26.06 ± 0.19	5351 ± 49
0.740	405	ALMA Band 8	35.32 ± 0.21	5242 ± 55
0.442	679	ALMA Band 9	107.20 ± 1.50	5678 ± 79

Table 2
Brightness Temperatures at Infrared Wavelengths for α Cen A from Liseau et al. (2013)

Wavelength (mm)	Frequency (GHz)	Facility	Flux (mJy)	Brightness Temperature (K)
0.870	345	LABOCA	28.00 ± 7	5738 ± 1432
0.500	600	Herschel-SPIRE	80 ± 30	5421 ± 2018
0.350	857	Herschel-SPIRE	145.00 ± 28	4822 ± 927
0.250	1199	Herschel-SPIRE	240.00 ± 50	4084 ± 845
0.160	1874	Herschel-PACS	560.00 ± 60	3920 ± 394
0.100	2998	Herschel-PACS	1410.00 ± 50	3909 ± 135
0.070	4283	Herschel-PACS	3350 ± 28	4540 ± 37
0.024	12491.5	Spitzer-MIPS	28530 ± 580	4736 ± 91

Table 2, we show additional observations of α Cen A. In the following subsections, we describe the set of tests used by KP.

6.1. Infrastructure for the Computations

For the following tests, we run KP in a single node of the cluster of the Center of Supercomputing of Space Weather of the National Laboratory of Space Weather in Mexico (LANCE). The node of the cluster has 40 threads with Intel Xeon E52670 v2 a 2.5 GHz, 128 GB of RAM (DDR3-1866), and 4 TB of storage. The operating system is Linux 4.2.0 SMP 64 bits.

6.2. Test of Auto-Convergence

Before starting these simulations with the real observed spectrum, we test the model using a synthetic spectrum produced by a solar atmosphere in hydrostatic equilibrium.

We use a set of radial profiles with variations of a pre-calculated atmosphere in equilibrium over the photosphere (z) as the input atmospheric model. We use the C7 model with variations in the temperature of -1000, -100, -10, $+10$, $+100$, and $+1000$ K as shown in Figure 2(a). We replace the observed spectrum used in this test with a synthetic spectrum computed with PakalMPI for the C7 model (test spectrum). The goal of replacing the observed spectrum is to keep the input and the output of the model under control.

KP successfully computed these models in around 3 hr using a single node with 28 threads (1 for each frequency). Table 3 show the frequencies and the computed synthetic spectrum used in this test.

In order to determinate the region where the emission is generated, in Figure 2(c) we include the normalized contribution function (CF) defined by

$$\mathrm{CF} = j_\nu \exp(-\tau_\nu), \tag{4}$$

where $j_\nu = \kappa_\nu B(T)$ and

$$\tau_\nu = \int \kappa_\nu dz, \tag{5}$$

are the optical depths. We found that our model computes the emission between 140 and 2120 km for 12.5 THz and 35 GHz, respectively. The gray regions in Figures 2(a)–(c) show the outer boundary of the model where the convergence method cannot be applied directly. On the other hand, the synthetic spectrum computed with these models fits the test spectrum (Figure 2(d)). The only result that did not converge completely to the initial condition is the $+1000$ K model (the segmented black line in Figure 2(b)). The auto-convergence test show that our methodology has an upper boundary for the initial condition of $+1000$ K.

In the following tests, we use the real spectrum of α Cen A with different restrictions in KP to understand the stability of the model.

6.3. Test without Restrictions (KP2019A)

In the second test, we use real observations of α Cen A using C7 as an input model without restrictions (i.e., the temperature model can take any value, even negative). KP makes 12,730 iterations in 49.5 hr in order to obtain the model KP2019A. The results are shown in Figures 3(a)–(b) as a dotted line. KP fixes the observed spectrum (Figure 3(a)) but the atmospheric model presents changes in the radial temperature that are very complicated to explain physically. The model shows the following characteristics: a high temperature at $\sim$1500 km over the photosphere $T_r > 11500$ K, negative temperatures at 1950 km, and abrupt changes of the temperature that reach values between 3×10^5 K and -2×10^5 K that are physically impossible. Analyzing the ray path of the solution of the radiative transfer equation in detail, we found that negative temperatures are due to Bremsstrahlung opacity. This opacity

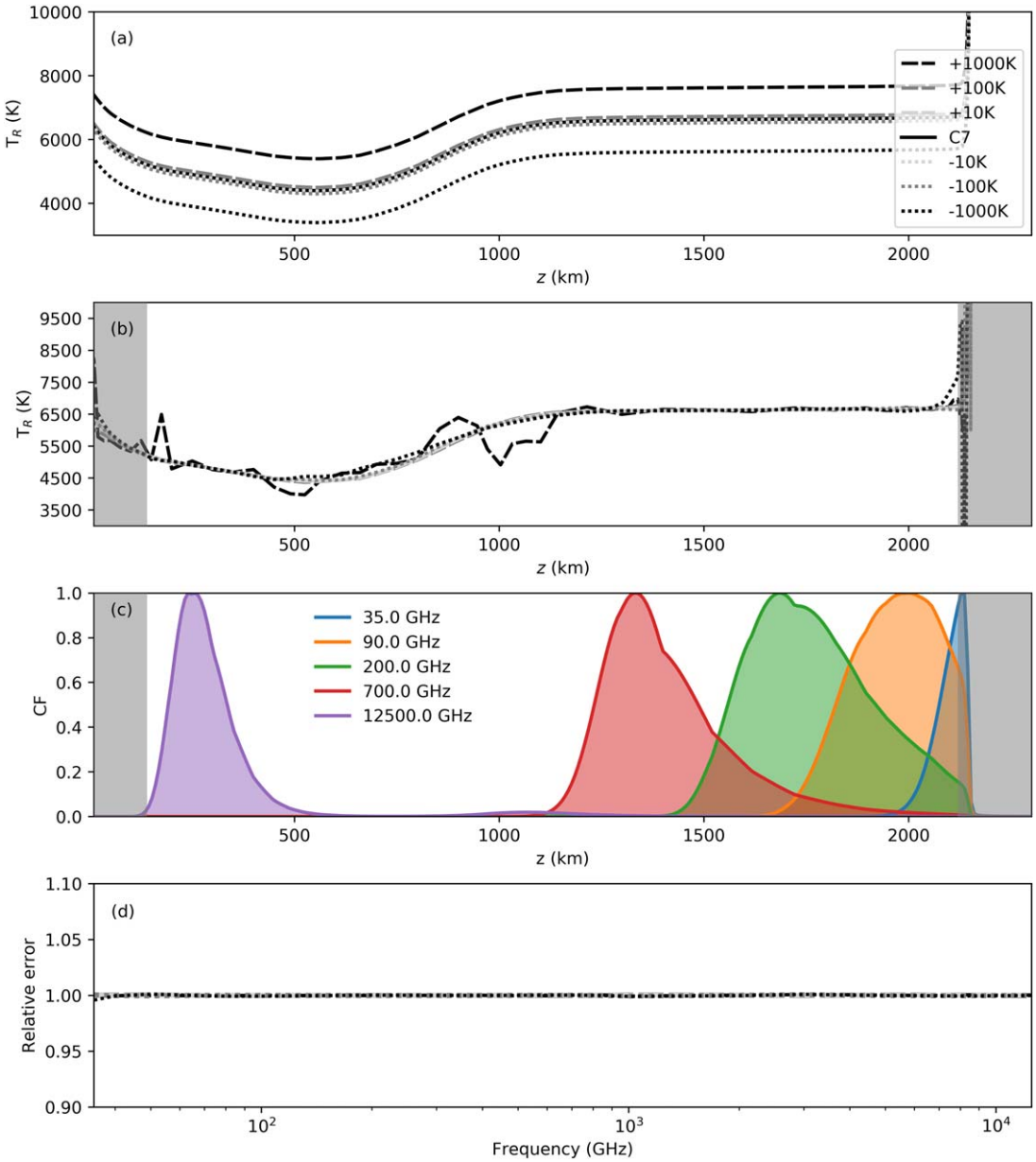

Figure 2. Convergence analysis using the C7 model for a set of initial conditions of the radial temperature profile with −1000, −100, −10, +10, +100, and +1000 K. (a) Set of models used as initial conditions for the chromosphere using the C7 model as a reference. (b) Radial temperature profile of each computed model in hydrostatic equilibrium. (c) Contribution functions of the C7 model for frequencies close to those observed by ALMA and *Spitzer*. (d) Relative error of the synthetic spectrum for each model taking the C7 model as a reference. All the models recover the C7 synthetic spectrum but the +1000 K model did not recover the radial temperature profile. The models +1000, −1000, and +100 K show negative values for the radial temperature at altitudes higher than 2130 km over the photosphere where the model cannot be applied (gray regions in panels (b)–(c)).

has the following form:

$$\kappa_\nu = C\frac{n_e n_i}{T^{3/2}}\nu^2,$$

where C is a constant, n_e is the electron density, n_i is the ion density, T is the temperature, and ν is the frequency. For temperatures less than 3000 K, the ion density of all the species that we study drops almost to zero ($n_i \approx 0$) because there is not enough energy to ionize the medium, especially hydrogen. That means that the atmosphere becomes optically thin. In other words, when the temperatures are higher than 2×10^4 K, if all the medium is practically ionized, then the opacity can be rewritten as

$$\kappa_\nu \approx C\frac{n_e^2}{T^{3/2}}\nu^2.$$

The n_e reaches a limit; however, the temperature can increase and, as a consequence, the opacity again drops to zero. In both cases: low and high temperatures imply an optically thin atmosphere ($\tau_\nu < 1$). These results show that solutions computed by KP in the radiative transfer equations without physical interpretations exist. In the following test, we constrain the minimum temperature in the solution to try to solve this feature of the model.

Table 3
Synthetic Spectrum between 35 GHz and 12.5 THz Processed by PakalMPI Using the C7 Model

Frequency (GHz)	Brightness Temperature (K)	Frequency (GHz)	Brightness Temperature (K)
35	7298	800	6600
40	7150	900	6591
50	6975	1000	6577
60	6878	2000	5918
70	6820	3000	5268
80	6781	4000	4982
90	6754	5000	4866
100	6734	6000	4823
200	6662	7000	4831
300	6641	8000	4838
400	6630	9000	4844
500	6621	10000	4854
600	6615	11000	4866
700	6608	12500	4886

6.4. Test Constraining Positive Temperatures (KP2019B)

In this test, we constrain the lower temperature limit in 3000 K. KP produced the KP2019B model after computing 11,300 models in around 44 hr. In the Figures 3(a)–(b), we show the results as dashed–dotted line. We observe that the computed spectrum does not exactly fix the observations of α Cen A (Figure 3(a)) like the last test. The radial temperature profile again shows temperatures without physical interpretations (Figure 3(b)). After 1600 km, the radial temperature increases suddenly with temperatures around 10^5 K.

6.5. Test with Bounded Temperatures (KP2019C)

We bounded the temperature taking both the initial model as a reference and the results of Section 6.2. We use the C7 model and a boundary of $\pm$1000 K to constrain. KP computed 7968 models in around 31 hr to produce our model called KP2019C. In Figures 3(a)–(b), we show the results as a dashed line. Figure 3(a) shows that the spectrum computed by KP is close to fitting the observed spectrum. However, we can observe that for low frequencies, the model does not exactly fix the observed spectrum. The temperature model (Figure 3(b)) shows similar a C7 model shape but with three main differences: (i) at photospheric altitudes, KP2019C shows a higher temperature than the C7 model; (ii) the temperature minimum of KP2019C is closer to the photosphere and shows a lower temperature of around 3200 K than the C7 model; and (iii) the temperature in the high chromosphere of KP2019C (after 1500 km) is higher than C7 by 1000 K. In the following test, we analyze the impact of the spatial resolution of the radial temperature profile.

6.6. Testing the Spatial Resolution (KP2019D)

The C7 model starts with 140 layers divided into three parts: the photosphere (20 layers), the chromosphere (81 layers), and the corona (39 layers), but in this test, we interpolate the model to increase the density four times in the chromospheric region up to 324 layers. KP2019D model is composed of 383 layers.

We used the same constraints as in Section 6.7. To calculate the final spectrum, KP computes 23,585 models in about 156 hr. The cyan solid lines in Figures 3(a)–(b) shows the results of the KP2019D model. In Figure 3(a), we plot the spectrum obtained by the model shown in Figure 3(b). We observe the same similarities of KP2019C but with changes in the temperatures with a more detailed spatial resolution. For example, the peak temperature of KP2019C at around 1000 km now is a set of spikes.

6.7. Smoothing Model (KP2019E)

We smooth the radial temperature profile from KP2019D using the Savitzky–Golay filter with a 9° polynomial (Savitzky & Golay 1964) to understand the effect of these spikes in the spectrum. This last profile was equilibrated again with PakalMPI to guarantee the hydrostatic equilibrium. The results are plotted in red in Figures 3(a)–(b). We called this model KP2019E.

In the model KP2019E, we eliminate the spikes and compute their synthetic spectrum using PakalMPI. In Figure 3(a), we observe the results of eliminating the spikes in the temperature model. At low frequencies, the spectrum has a better fix. At frequencies lower than 300 GHz, the spectrum does not fix exactly the observations but are inside of the observations error limits for all the points of the spectrum, except at 700 GHz, which corresponds to the Band 9 of ALMA. This observation is the responsible of the increase of temperatures in the radial profile between 450 and 1100 km over the photosphere. The model KP2019E shows a continued profile without spikes. The temperature minimum is lower ($\sim$3000 K) and closer to the photosphere ($\sim$500 km) than the C7 model. The radial temperature of KP2019E after 1500 km is higher than the C7 model.

In Figure 3, we show the results of computing the CF (panel (c)) and the optical depth (panel (d)) for the KP2019E model at 35, 97.5, 233, 679, and 12491.5 GHz. We found that for the case of 12491 GHz, the CF has a maximum at altitudes closed to 250 km over the photosphere. For the other cases, the CF shows three peaks at 679 GHz, two peaks at 233 GHz, and one peak at 97.5 and 35 GHz. These peaks in the CF shows similarities with the reported solar CF (Selhorst et al. 2019) that show two peaks (around 230 GHz) and one peak (around 100 GHz).

7. Discussion and Conclusions

In this work, we present KP, which is a nonlinear method to compute a stellar atmosphere to fix an observed and synthetic spectrum through a semiempirical model of the chromosphere at millimeter, submillimeter, and infrared wavelengths. KP uses the LM algorithm to minimize the differences between synthetic and observed spectrum by running PakalMPI to hydrostatically equilibrate the atmosphere and to compute their synthetic spectrum. KP uses MPI libraries, C, and Julia Languages to solve the model in parallel where it is possible to divide the computations.

We test the auto-convergence of the method using a set of variations from the C7 model and found that variations greater than $+$1000 K over the profile impact the final radial temperature model. This numerical behavior shows that the initial conditions should be lower than $+$1000 K over the final solution. We cannot directly compute stars with a spectral class far to the solar-like classification. Computations with small variations in the radial temperature profile able reproduce their emission is mandatory, especially for stars colder than the Sun. We used the radial density of the C7 model as an initial

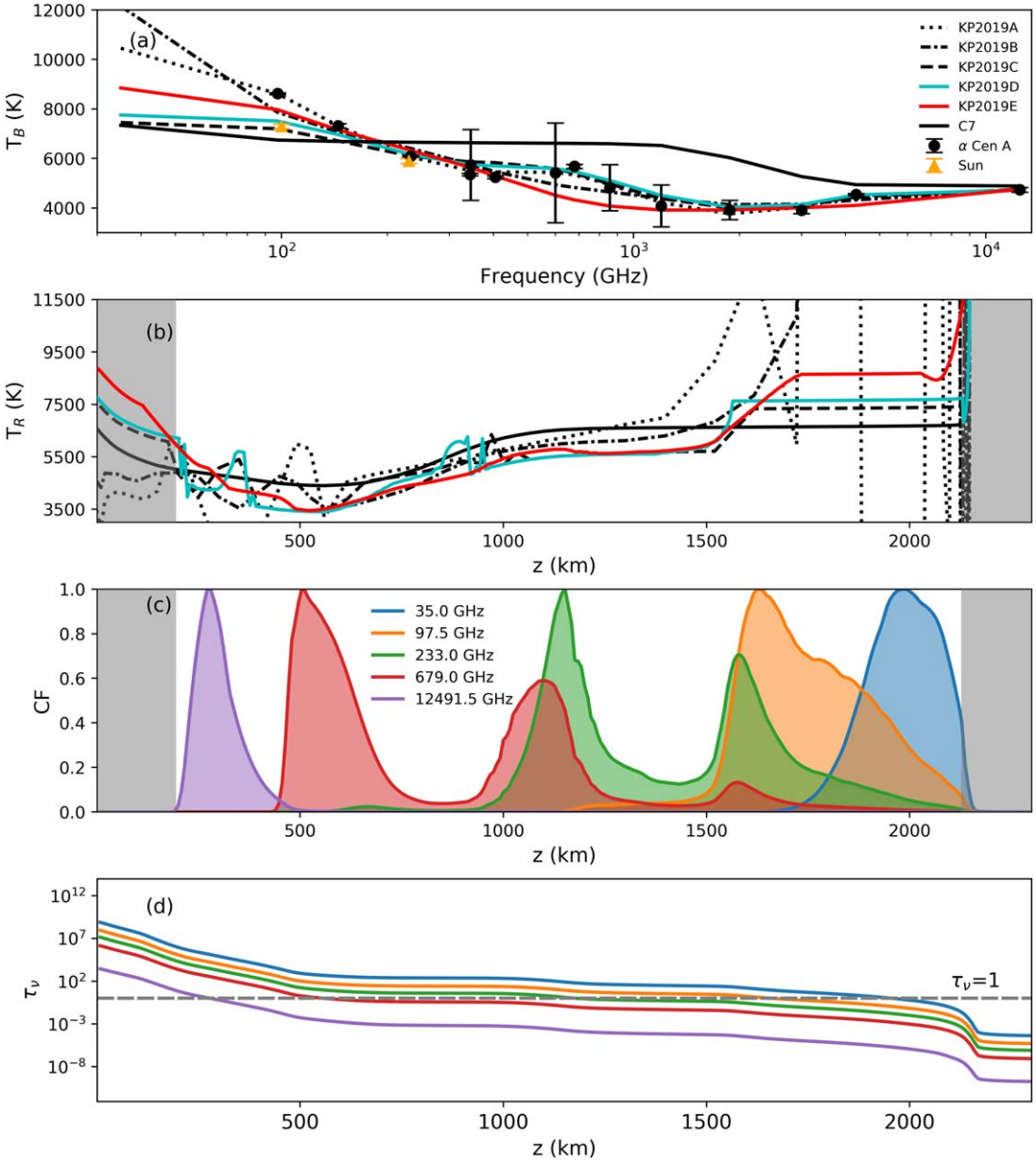

Figure 3. α Cen A model obtained from KP. (a) The dotted line shows the model KP2019A without restrictions. The dotted–dashed line presents the KP2019B model with positive temperatures restriction. The dashed line is KP2019C model with a bounded temperature. The cyan solid line indicate the synthetic spectrum from the raw temperature profile (KP2019D model). The red solid line is the synthetic spectrum after smoothing (KP2019E model). The solid black line is the synthetic spectrum of the C7 solar model. The circle markers are observations of α Cen A from Liseau et al. (2016, 2013), and the triangle markers are the Sun observations from ALMA (White et al. 2017). (b) Radial temperature profiles over the photosphere. We show that the radial temperature for α Cen A between 290 and 1560 km is lower than the solar model. In the outer boundary, the temperature remains higher than in the solar model. (c) Normalized CF of the KP2019E model of α Cen A for the same frequencies. For the case of 12491 GHz, we found that the CF has a maximum close to 250 km over the photosphere. For the other cases, the CF shows three peaks for 679 GHz, two peaks for 233 GHz, and one peak for 97.5 GHz and 35 GHz. (d) Optical depth for 35 GHz, 97.5 GHz, 233 GHz, 679 GHz, and 12491.5 GHz for the KP2019E model of α Cen A.

condition for all the simulations. However, Figure 2(c) show that for low frequencies, the CF is truncated due to low density at this altitude. In order to fix the CF, a wider chromosphere than the C7 model's density is required.

In this context, we use spectral observations of α Cen A at millimeter, submillimeter, and infrared wavelengths and the C7 semiempirical model as an input model with the following constraints: without restrictions, limiting the lower temperature, and bounding the temperature profile. We found that the solution of KP is acceptable only in the regimen of the "bounding temperature" as shown in the model KP2019D. A detailed simulation using greater spatial resolution shows that the shape of the profile is preserved, but the profile shows several spikes that are numerical artifacts in the radial temperature profile. These spikes are related to the increase in the brightness temperature in some points of the observed spectrum, specifically at Band 3 (97.5 GHz) and 9 (679 GHz) of ALMA.

We eliminate the spikes using the filter of Savitzky–Golay with a polynomial of nine degree. We compute the hydrostatic

equilibrium of this last profile and called to this model KP2019E. The synthetic spectrum obtained from KP2019E fixed all the observed points inside of their observational errors for α Cen A except band 3 and 9 of ALMA. The spectrum computed from KP2019E suggest that both bands presents an over flux in agreement with the analysis of Liseau (2019).

The CF for frequencies at 35 GHz, 97.5 GHz, 233 GHz, 679 GHz, and 12491.5 GHz (ALMA and *Spitzer* coverage, Figure 3(c)) shows similarities (one peak of CF at 100 GHz and two peaks at 230 GHz) in comparison with the solar models (Selhorst et al. 2019). In the KP2019E model, the maximum peaks for the aforementioned frequencies occurs at a height of 2140, 1625, 1150, 510, and 275 km, which corresponds with the distance over the stellar photosphere where $\tau_\nu \approx 1$ (Figure 3(d)).

The results obtained by the methodology here are presented to show that KP is capable of finding the physical conditions of stellar atmospheres of Solar-like stars using their observed spectra at millimeter, submillimeter, and infrared wavelengths. We show that KP is a stable and fast method that can compute thousands of atmospheres in a few hours.

The impact of the radial density as an initial condition in the computation of the radial temperature profile as well as the estimation of a wider solar chromosphere using our methodology is considered for future work. KP can be provided upon request to the authors.

The authors thank the referee for helpful and valuable comments on this paper. This work was supported by the Ciencia Básica (254497) CONACyT Fellowship.

ORCID iDs

F. Tapia-Vázquez https://orcid.org/0000-0001-9132-7196
V. De la Luz https://orcid.org/0000-0003-0257-4158

References

Avrett, E. H., & Loeser, R. 2008, ApJS, 175, 229
Carlsson, M. 1992, in ASP Conf. Ser. 26, Cool Stars, Stellar Systems, and the Sun, ed. M. S. Giampapa & J. A. Bookbinder (San Francisco, CA: ASP), 499
Cayrel de Strobel, G. 1996, A&ARv, 7, 243
Cranmer, S. R., Wilner, D. J., & MacGregor, M. A. 2013, ApJ, 772, 149
De la Luz, V. 2016, ApJ, 825, 138
De la Luz, V., Chavez, M., Bertone, E., et al. 2014, SoPh, 289, 2879
De la Luz, V., Lara, A., Mendoza-Torres, J. E., et al. 2010, ApJS, 188, 437
De la Luz, V., Lara, A., & Raulin, J.-P. 2011, ApJ, 737, 1
Dere, K. P., Landi, E., Mason, H. E., et al. 1997, A&AS, 125, 149
Dulk, G. A. 1985, ARA&A, 23, 169
Fontenla, J. M., Avrett, E., Thuillier, G., et al. 2006, ApJ, 639, 441
Fontenla, J. M., Avrett, E. H., & Loeser, R. 1993, ApJ, 406, 319
Golovinskii, P. A., & Zon, B. A. 1980, ZhTFi, 50, 1847
Güdel, M. 2002, ARA&A, 40, 217
Kervella, P., Bigot, L., Gallenne, A., et al. 2017, A&A, 597, A137
Kudaka, A. S., Cassiano, M. M., Marcon, R., et al. 2015, SoPh, 290, 2373
Linsky, J. L. 2017, ARA&A, 55, 159
Liseau, R. 2019, arXiv:1904.03043
Liseau, R., De la Luz, V., O'Gorman, E., et al. 2016, A&A, 594, A109
Liseau, R., Montesinos, B., Olofsson, G., et al. 2013, A&A, 549, L7
Liseau, R., Vlemmings, W., Bayo, A., et al. 2015, A&A, 573, L4
Loukitcheva, M., Solanki, S. K., Carlsson, M., et al. 2004, A&A, 419, 747
Machado, M. E., Avrett, E. H., Vernazza, J. E., et al. 1980, ApJ, 242, 336
Marquardt, D. W. 1963, J. Soc. Industrial Appl. Math., 11, 431
Mogensen, P. K., & Riseth, A. N. 2018, JOSS, 3, 615
Nakajima, H., Nishio, M., Enome, S., et al. 1995, JApAS, 16, 437
Press, W. H., Flannery, B. P., & Teukolsky, S. A. 1986, Numerical Recipes: The Art of Scientific Computing (Cambridge: Univ. Press)
Pujol, J. 2007, Geop, 72, W1
Savitzky, A., & Golay, M. J. E. 1964, AnaCh, 36, 1627
Selhorst, C. L., Simões, P. J. A., Brajša, R., et al. 2019, ApJ, 871, 45
Trottet, G., Raulin, J.-P., Mackinnon, A., et al. 2015, SoPh, 290, 2809
Vernazza, J. E., Avrett, E. H., & Loeser, R. 1976, ApJS, 30, 1
Vernazza, J. E., Avrett, E. H., & Loeser, R. 1981, ApJS, 45, 635
Wedemeyer, S., Bastian, T., Brajša, R., et al. 2016, SSRv, 200, 1
White, S. M., Iwai, K., Phillips, N. M., et al. 2017, SoPh, 292, 88
Zheleznyakov, V. V. 1996, ASSL, 204